Research Report

A New Isolated Multi-port Converter Using Interleaving and Magnetic Coupling Inductor Technologies

Masanori Ishigaki, Kenichi Ito, Shuji Tomura and Takaji Umeno

Report received on Nov. 8, 2013

ABSTRACT This paper proposes a new multi-port converter with interleaved magnetic coupling technologies. With the focus on the impedance behavior of coupled magnetic components and the control parameters, this multi-port converter integrates one isolated dc-dc converter and two multi-phase boost converters, and controls these topologies independently. The proposed converter has the capability to connect four dc applications or sources in total, and so brings significant cost reduction and improves the total loss consumption of power systems. In addition, magnetic isolation brings high reliability of complex power systems such as electric vehicles or grid-connected industries. In this paper, the basic circuit behavior is verified by theoretical considerations and experiments. An example of the proposed circuit as a multifunctional dc power system is demonstrated with the simulation results. Such an approach could bring about variable application fields to dc electric power systems.

KEYWORDS Power Electronics, Dc-Dc Converter, Multi-port, Power Semiconductor, Magnetic Devices, Electrical Vehicle, Grid Connected Industries

1. Introduction

With the rapid development of energy storage device technologies, dc power systems are becoming widely used in various applications. In electricity infrastructures, large energy storage devices such as Li-ion and NaS batteries promote distributed renewable energy sources, which include photovoltaic power systems, wind generator systems, and fuel cell systems in micro grids.[1,2] In vehicles, gas-electric hybrid vehicles are becoming mainstream all over the world, and with further development of the power/energy densities of batteries, plug-in or purely electric vehicles can also become mainstream in future transportation systems.[3,4,14-16] As energy storage device technologies progress, the electric systems become more complex. Therefore, cost reduction and downsizing of dc-dc converter circuits is actively sought as a common goal for power conversion circuits. To achieve this goal, power electronics technologies are developing new semiconductor devices such as SiC and GaN.[5–8] In other approaches, inventions of circuit topologies have been used with some success for cost reduction and weight saving of complex dc power systems. [9-13]

This paper proposes a new multi-port converter capable of controlling four dc components. With magnetic coupling technologies, the proposed circuit achieves integration of two multi-phase boost converters and one isolated dc-dc converter in one circuit. By controlling the duty and phase of each switch, it is possible to control voltages and transfer isolated dc power independently. In this paper, the basic functions and design of magnetic components are shown with a theoretical analysis. Then, the static characteristics and conversion efficiency are verified with experimental results. The simulation results demonstrate the application to an electric vehicle.

2. Electrical Vehicle System and Issues

2. 1 Basic System Configuration

Figure 1 shows an example of the basic power system of an electric vehicle. This electric vehicle system mainly consists of a motor MG, a large capacity and high-voltage main battery $BATT_m$ for driving, and a low voltage system battery $BATT_S$ for ensuring a stable supply of power to computer elements and other important subsystems. Generally, a conventional lead battery is the system battery $BATT_S$, and the voltage is typically V_{Bs} = 12 – 14 V. Depending on the vehicle

system specification, the voltage of the main battery V_{Bm} is set as V_{Bm} = 100 – 500 V. Often, the system battery V_{Bm} is set as 100 – 200 V, with a connect boost "CONVERTER A" between the battery $BATT_m$ and the motor MG to improve the motor efficiency and the controlled performance.[14-17] For the same reason, electrical connections using "CONVERTER B" are used between the system battery $BATT_S$ and the load of high-power actuators $LOAD_b$.[4] Additionally, the main battery $BATT_m$ and the system battery $BATT_S$ are interconnected by an isolated dc-dc converter "CONVERTER C" for hardware redundancy and fail-safe design. The main battery $BATT_m$ needs to be charged from an external AC or DC power supply, EXT_{AC} or EXT_{DC}, through the battery charger circuit "CHARGER".

2. 2 Standard Circuit Schematics and Functions

Figures 2 and **3** show conventional converter circuits and ideal waveforms.[18–20] Figure 2(a) is an interleaved multi-phase converter circuit using "CONVERTER A" and "CONVERTER B", shown in Fig. 1. The two inductors L_{b1} and L_{b2} can be directly or inversely coupled by constructing directional selections between the two windings. In this case, L_{b1} and L_{b2} are an inverse coupling with coupling coefficient k_b. Figure 3(b) shows the ideal waveforms of the interleaved multi-phase converter. The phase between V_u and V_v is set as π, and the duty ratio is set as $D = \delta_d/2\pi$. In this configuration, the voltage relationship between input voltage V_i and output voltage V_o is given by

$$V_o = \frac{1}{1-D} V_i \tag{1}$$

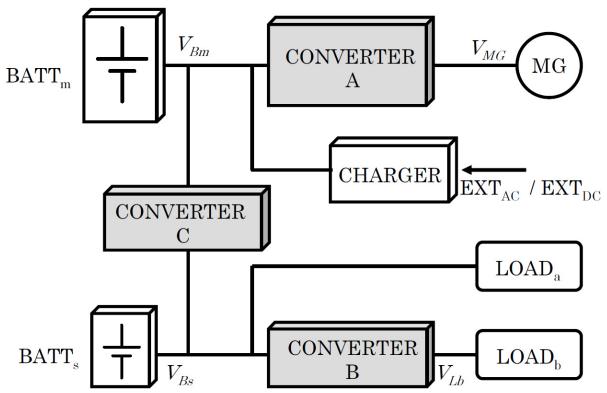

Fig. 1 Basic system of an electric vehicle. Two batteries and three loads are connected to three converters in this example.

The output voltage V_o is controlled by adjusting the duty ratio D. In each period, the derivative value of the input current i'_{in} and the inductor current i'_{Lb1} can be described in

$$i'_{in}[\theta_1 \le \theta \le \theta_2] = -\frac{1}{(1+k_b)L_b}(V_o - 2V_i) \tag{2}$$

$$i'_{in}[\theta_2 \le \theta \le \theta_3] = \frac{2}{(1+k_b)L_b} V_i \tag{3}$$

$$i'_{Lb1}[\theta_1 \le \theta \le \theta_2] = -\frac{1}{1-k_b^2}\frac{V_o}{L_b} + \frac{1}{1+k_b}\frac{V_i}{L_b} \tag{4}$$

$$i'_{Lb1}[\theta_2 \le \theta \le \theta_3] = \frac{1}{(1+k_b)L_b} V_i \tag{5}$$

Because of the inversely coupled effect, the current ripple of i_{Lb1} is a monotonically increasing function of k_b. Thus, the core and winding losses of the inductors increase with increasing k_b. In contrast, the switching losses decrease drastically if the boost converter operates in the discontinuous current mode, when i_{Lb1} across zero is $\theta = \theta_2$. Therefore, the total efficiency can be optimized to select the parameters L_b and k_b by considering the steady-state duty, the power ratio, and characteristics of the magnetic components and the semiconductors.

Figure 2(b) is an isolated dc-dc converter circuit using "CONVERTER C", shown in Fig. 1.[21-23] The primary bridge S_{d1} – S_{d4} and the secondary bridge

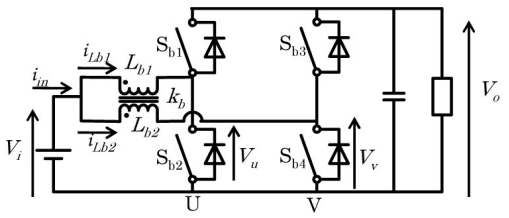

(a) Interleaved multi-phase boost converter

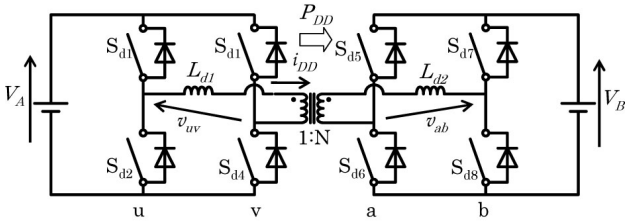

(b) Bi-directional isolated dc-dc converter

Fig. 2 Conventional converter circuits. Because of its high efficiency and response, the multi-phase type boost converter (a) is widely accepted. Due to the large capacity of transferred power, the standard circuitof the bi-directional isolated dc-dc converter is the full-bridge type (b).

S_{d5} – S_{d8} are connected through inductors L_{d1}, L_{d2}, and transformer Tr with turn ratio 1: N. Figure 3(b) shows the ideal waveforms of the bi-directional isolated dc-dc converter. The adjusted phase angle between the primary and the secondary inductor currents is ϕ_d, and the duty ratio of each bridge is set as D = 1/2. In the period $\theta_1 \leq \theta \leq \theta_2$, the derivative value of the primary inductor current i'_{dd} is as follows:

$$i'_{dd} = \frac{V_A + V_B/N}{L_{DD}} \quad (6)$$

$$L_{DD} = L_{d1} + L_{d2}/N^2 + L_l \quad (7)$$

where L_l is the primary equivalent value of the leakage inductance of the transformer. The transmitted power P_{DCDC} is given by

$$P_{DCDC} = \frac{V_A V_B}{\omega_s L_{DD}} \left(\phi_d - \frac{\phi_d^2}{\pi} \right) \quad (8)$$

According to Eq. (8), the P_{DCDC} applies control by adjusting the phase angle ϕ_d.

In the case of Fig. 1, the number of semiconductors and magnetic components is equal to 21, and these thus lead to issues of cost, volume, and productivity of converters.

3. Proposed Multi-port Converter

Figure 4 shows the proposed multi-port converter. Figure 4(a) is the circuit schematic, which shows two full-bridge inverters and three magnetic components constructing four dc ports (port A– port D). Figure 4(b) shows the structure of the magnetic components of Fig. 4(a). The magnetic components consist of three cores: one is for the transformer, and the other two are for the inductors L_u – L_b. The parameters of the magnetic components must be symmetric, the number of windings is 1:1:n:n, and the inductance is $L_u = L_v$, $L_a = L_b$. To simplify the theoretical analysis, the magnetic coefficients are set as $k_1 = k_2 = k$. Each winding of the transformer has a center tap that makes port C and port D such that primary ports A and C, and secondary ports B and D are connected by the multi-phase boost converter, as shown in **Fig. 5**(a), and ports A and B are connected by the isolated dc-dc converter, as shown in Fig. 5(b). Thus, all four ports A – D are connected bi-directionally. The primary inductors L_u, L_v and the secondary inductors L_a, L_b are strongly inversely coupled inductors connected to each winding of the transformer. Consequently, the number of magnetic components and semiconductors is reduced by more than half of that of the conventional system example described in Section 2.

In the theoretical analysis of this converter, it is

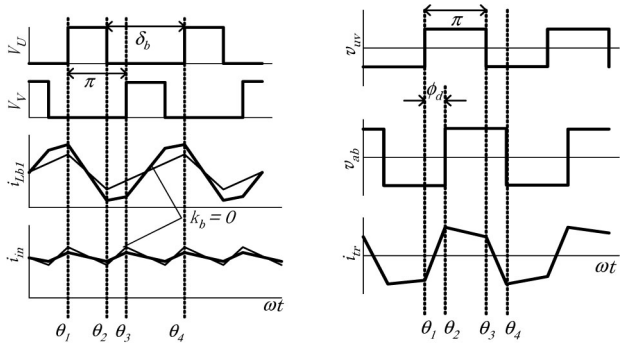

(a) Ideal waveforms of the interleaved multi-phase converter

(b) Ideal waveforms of the bi-directional isolated dc-dc converter

Fig. 3 Ideal waveforms of convenional circuits. The boost converter controlled duty angle is $delta_b$, and the dc-dc converter is controlled by phase angle ϕ_d.

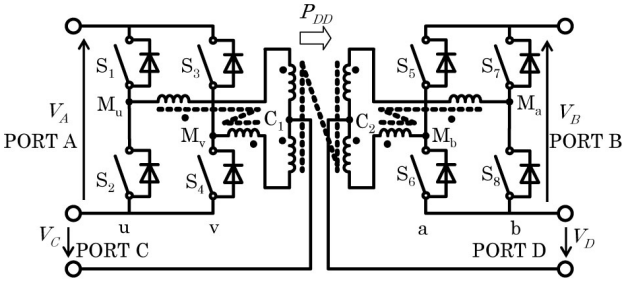

(a) Schematic of the proposed circuit

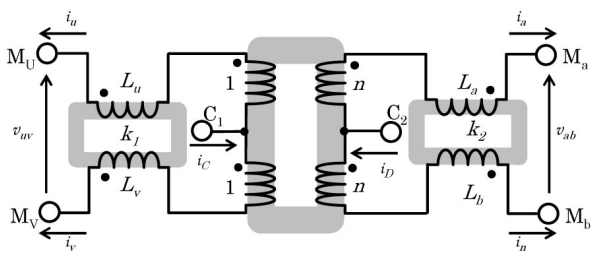

(b) Detail of magnetic components

Fig. 4 The proposed multi-port converter. Major parts of the proposed converter are the same as the isolated dc-dc conterter, but center-tapped C_1, C_2 of the transformer adds two more ports.

important to understand the behavior of the magnetic components. **Table 1** shows the impedance behavior of the magnetic components, the impedance of the inversely coupled inductors, the increase against the common mode current, and the decrease against the differential mode current. As indicated in this table, the inductors work as large inductance L_b in Eqs. (4) and (5) for the boost converter function, and also work as small inductance L_{DD} in Eq. (8) for the isolated dc-dc converter function. The exiting inductance of the transformer is canceled against the common mode current, and so the transformer only works as a differential current, so that no interference exists between the two functions.

Figures 6 and **7** show examples of the ideal waveforms and equivalent circuits of the proposed converter. To control multi-phase boost operation, the duty ratio of all lower switches is adjusted as $D = \delta/2\pi$, and the phase angles between V_U and V_V, V_A and V_B are set as π. By using the same principle of the isolated dc-dc converter illustrated in Fig. 2(b), the phase angle between primary voltage v_{uv} and secondary voltage v_{ab} is the adjusted ϕ. The behavior of the proposed converter becomes different with each change in the relationship between the duty angle δ and the phase angle ϕ. Figures 6(a) and 7(a) show the ideal waveforms and equivalent circuits in the case of $\delta \geq \pi + \phi$. In Fig. 7, all descriptions are shown as the primary side, and the arrows indicate the current direction of each period. For example, in periods I and II, the input current i_C is increased and the common current is through the inversely coupled inductors L_u and L_v. Aside from this, the differential current is through L_u and L_v by secondary voltage v_B / N, and the transformer current i_{DD} increases in period I. In period II, the common current is through the transformer from V_C but its own exciting is canceled, so that no interference or magnetic saturation occurs in this converter. Figures 6(b) and 7(b) show the ideal waveforms and equivalent circuits in the case of $\delta \leq \pi + \phi$. In Fig. 6(b), the transformer exited as $\pm (V_A + V_B / N)$ in period 2 ($\theta_2 \leq \theta \leq \theta_3$) and period 6 ($\theta_6 \leq \theta \leq \theta_7$), so the shape of transformer current i_{DD} is a different waveform in Fig. 6(a).

Tables 2 and **3** show the derivative values of i_u and i_v

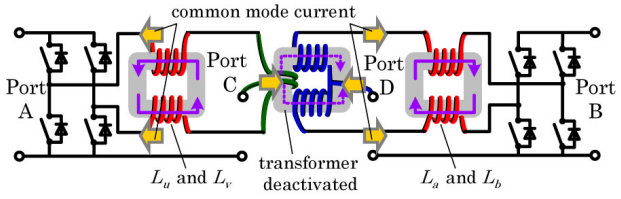

(a) Boost converter function

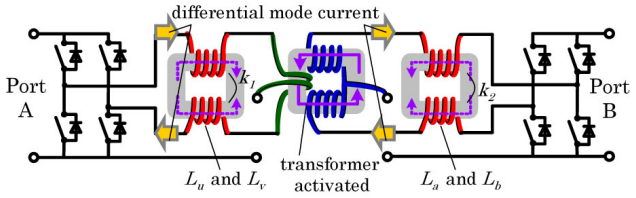

(b) Isolated dc-dc converter function

Fig. 5 Illustration of the basic functions of the proposed converter. Due to the directions of the windings, the flux of the magnetic components in each function is distinct.

Table 1 Impedance behavior of inversely coupled inductor and transformer.

Current direction in Fig. 5	Primary inductance of coupled inductor	Secondary inductance of coupled inductor	Exciting inductance of transformer
Common	$2L_u(1+k_1)$	$2L_a(1+k_1)$	zero (canceled)
Differential	$2L_u(1-k_1)$	$2L_a(1-k_1)$	large (excited)

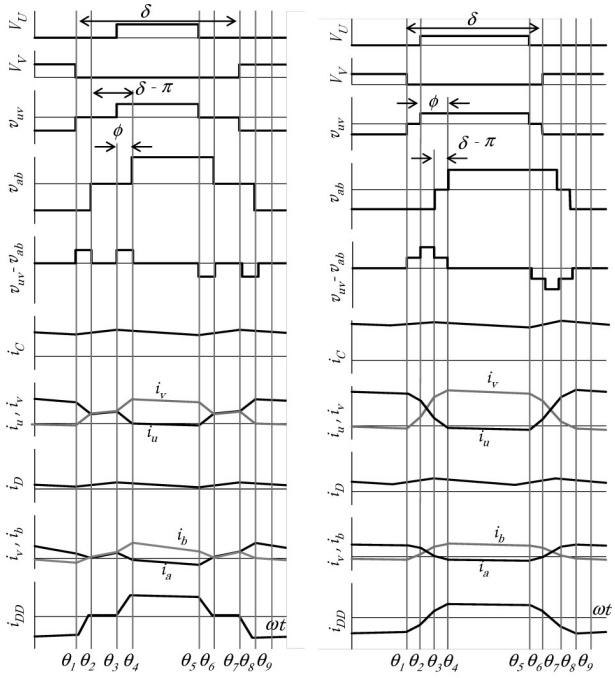

(a) $0 \leq \phi \leq \delta - \pi$ (b) $0 \leq \delta - \pi \leq \phi$

Fig. 6 Ideal waveforms of the proposed circuit.

in each period of Fig. 7(a) and 7(b). Due to symmetry, these tables describe only a half period of Fig. 7, and for simplicity, the voltage is set as $V_A = V_B / N$. Here L_s is comparable to L_{DD} in Fig. 2(b) and is given by

$$L_s = L_u + \frac{L_a}{N^2} \tag{9}$$

According to Table 2 and 3, the common mode current $i_{cm} = i_C$ has the same value as that of the conventional boost converter in Eqs. (2) and (3). Therefore, the proposed converter makes it possible to control voltages by adjusting the duty ratio D. However, due to the differential mode current i_{df} through the transformer, the isolated dc-dc power P_{DD} is transferred between port A and port B. The transfer power P_{DD} can be calculated by

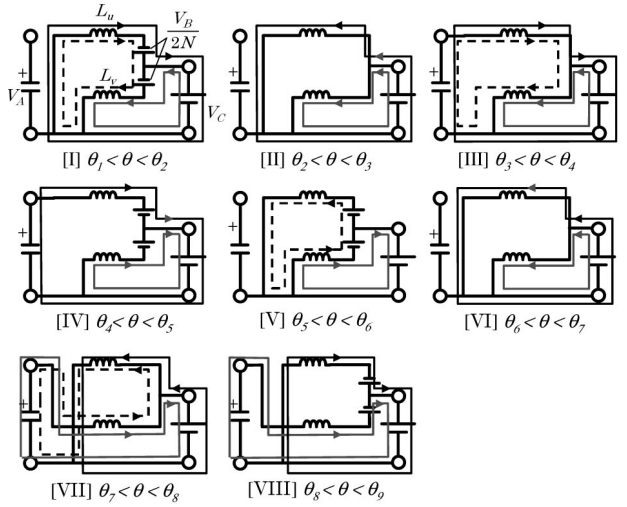

(a) Equivalent circuits of Figure 6(a).

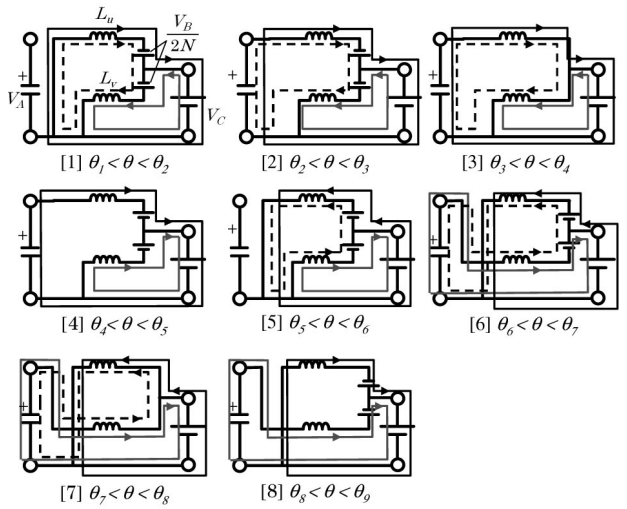

(b) Equivalent circuits of Figure 6(b).

Fig. 7 Equivalent circuits and functions of Fig. 6.

$$P_{DD} = \frac{V_A V_B}{\omega \{2(1-k)L_s + L_l\} N} \frac{1}{\pi} \times f(\delta, \phi) \tag{10}$$

$$f(\delta,\phi) = \delta(\pi - \delta) \quad : [0 \le \delta \le |\phi|] \tag{11}$$

$$= \phi(\delta - \phi) \quad : [|\phi| \le \delta \le \pi] \tag{12}$$

$$= \phi(\pi - \phi) + (\delta - \pi)^2 \quad : [\pi \le \delta \le \pi + |\phi|] \tag{13}$$

$$= \phi(2\pi - \delta - \phi) \quad : [\pi + |\phi| \le \delta] \tag{14}$$

By using Eq. (10), P_{DD} is expressed as a function of ϕ and δ, and variables L_u, L_v, L_a, L_b, and k.

4. Experimental Results

4. 1 Experimental Verifications

The experimental configuration is shown in **Fig. 8** and **Table 4**. The voltage of the input dc source of port D is set as $V_D = 100$ V, and load R_v is connected to port B. Port A and port C have contactors SW_A and SW_B for choosing either primary power source V_A or V_C. All switching devices are MOSFET (IXFN130N30, 300 V, 130 A, IXYS), and the core material of the transformer and the inductors is Finemet (F3CC0025, Hitachi). The turn ratio of the transformer is set as $N = 5$, and the number of primary windings is $n_1 = n_2 = 2$.

Table 2 Derivative values of i_u and i_v in Fig. 7(a).

	i'_u	i'_v	$i'_{cm} = i'_u + i'_v$	$i'_{df} = \frac{i'_v - i'_u}{2}$
I	$-\frac{1+k}{2(1-k^2)}\frac{V_A}{L_s} + \frac{1-k}{1-k^2}\frac{V_C}{L_s}$	$\frac{1+k}{2(1-k^2)}\frac{V_A}{L_s} + \frac{1-k}{1-k^2}\frac{V_C}{L_s}$	$\frac{2}{1+k}\frac{V_C}{L_s}$	$\frac{1}{1-k}\frac{V_A}{2L_s}$
II	$\frac{1}{(1+k)L_s}V_C$	$\frac{1}{(1+k)L_s}V_C$	$\frac{2}{1+k}\frac{V_C}{L_s}$	0
III	$-\frac{1}{1-k^2}\frac{V_A}{L_s} + \frac{1}{1+k}\frac{V_C}{L_s}$	$\frac{k}{1-k^2}\frac{V_A}{L_s} + \frac{1}{1+k}\frac{V_C}{L_s}$	$-\frac{1}{1+k}\frac{V_A}{L_s} + \frac{2}{1+k}\frac{V_C}{L_s}$	$\frac{1}{1-k}\frac{V_A}{2L_s}$
IV	$-\frac{1}{2(1+k)}\frac{V_A}{L_s} + \frac{1}{1+k}\frac{V_C}{L_s}$	$-\frac{1}{2(1+k)}\frac{V_A}{L_s} + \frac{1}{1+k}\frac{V_C}{L_s}$	$-\frac{1}{1+k}\frac{V_A}{L_s} + \frac{2}{1+k}\frac{V_C}{L_s}$	0

Table 3 Derivative values of i_u and i_v in Fig. 7(b).

	i'_u	i'_v	$i'_{cm} = i'_u + i'_v$	$i'_{df} = \frac{i'_v - i'_u}{2}$
1	$-\frac{1+k}{2(1-k^2)}\frac{V_A}{L_s} + \frac{1-k}{1-k^2}\frac{V_C}{L_s}$	$\frac{1+k}{2(1-k^2)}\frac{V_A}{L_s} + \frac{1-k}{1-k^2}\frac{V_C}{L_s}$	$\frac{2}{1+k}\frac{V_C}{L_s}$	$\frac{1}{1-k}\frac{V_A}{2L_s}$
2	$-\frac{1}{1+k}\frac{V_A}{L_s} + \frac{1}{1+k}\frac{V_C}{L_s}$	$-\frac{1}{1+k}\frac{V_A}{L_s} + \frac{1}{1+k}\frac{V_C}{L_s}$	$\frac{2}{1+k}\frac{V_C}{L_s}$	$\frac{2}{1-k}\frac{V_A}{2L_s}$
3	$-\frac{1}{1-k^2}\frac{V_A}{L_s} + \frac{1}{1+k}\frac{V_C}{L_s}$	$\frac{k}{1-k^2}\frac{V_A}{L_s} + \frac{1}{1+k}\frac{V_C}{L_s}$	$-\frac{1}{1+k}\frac{V_A}{L_s} + \frac{2}{1+k}\frac{V_C}{L_s}$	$\frac{1}{1-k}\frac{V_A}{2L_s}$
4	$-\frac{1}{2(1+k)}\frac{V_A}{L_s} + \frac{1}{1+k}\frac{V_C}{L_s}$	$-\frac{1}{2(1+k)}\frac{V_A}{L_s} + \frac{1}{1+k}\frac{V_C}{L_s}$	$-\frac{1}{1+k}\frac{V_A}{L_s} + \frac{2}{1+k}\frac{V_C}{L_s}$	0

The primary inductance is set as $L_u = L_v = 10\ \mu$H, secondary inductance is set as $L_a = L_b = 50\ \mu$H, and both coupling coefficients are $k_1 = k_2 = 0.8$. Given this specification, the switching frequency is set as 20 kHz.

Figures 9 and **10** illustrate the result of steady-state operations. In this condition, dc power is transferred form port C to port A by using the boost converter. This power is transferred to port B by using the isolated dc-dc converter, and finally reaches port D by using the down conversion. Thus, the transferred power is described as $P_{DD} = i_C V_C$. In Fig. 9, the experimental waveforms in three cases of duty ratio D are shown. The voltages V_A and V_B are estimated from the output voltages of each bridge, v_{uv} and v_{ab}: $V_A = 32$ V, $V_B = 165$ V at $D = 0.4$, $V_A = 40$ V, $V_B = 200$ V at $D = 0.5$, $V_A = 50$ V, $V_B = 250$ V at $D = 0.6$, and the result shows the boost converter function follows Eq. (1). The inductor current i_u is shaped like traperized, biased half of i_C. The input current i_C shape is nearly flat due to the effect of multiphase boost conversion, and the average value is increased monotonously by duty ratio D. In Fig. 10, the experimental results of transferred power P_{DD} are compared with estimated values from Eq. (10) and Table 4. The experimental values correspond to the estimated lines, controlled by phase angle ϕ and duty ratio D.

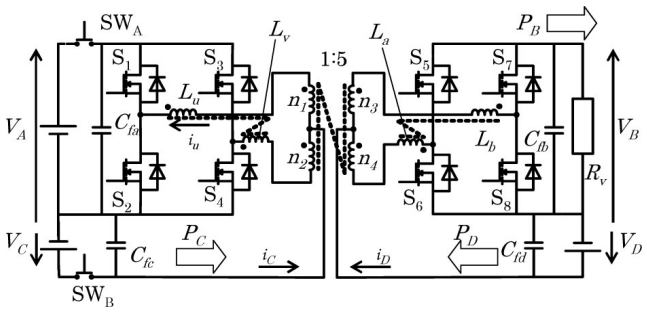

Fig. 8 Setup of the experimental circuit.

Table 4 Circuit parameter of the experimental circuit.

Parameter	Symbol	Value
Rated power	P_{DD}	±800 W
Rated input voltage	V_A, V_C, V_D	50 V, 20 V, 100 V
Rated Duty	D	0.2 ~ 0.8
Turn ratio of transformer	N	1:5
Turn number of transformer	n_1	2
Magnetizing inductance (primary)	L_m	310 μH
Coupling coefficient of transformer	k_{tr}	0.98
Coupled inductor (primary)	L_u, L_v	10 μH
Coupling inductor (secondary)	L_a, L_b	50 μH
Coupling coefficient of inductor	k	0.8
Core material of inductor and transformer		Finemet (Hitachi material)
dc capacitor	C_f	1400 μF
Dead time	T_d	1 μs
Switching frequency	f_{sw}	20 kHz

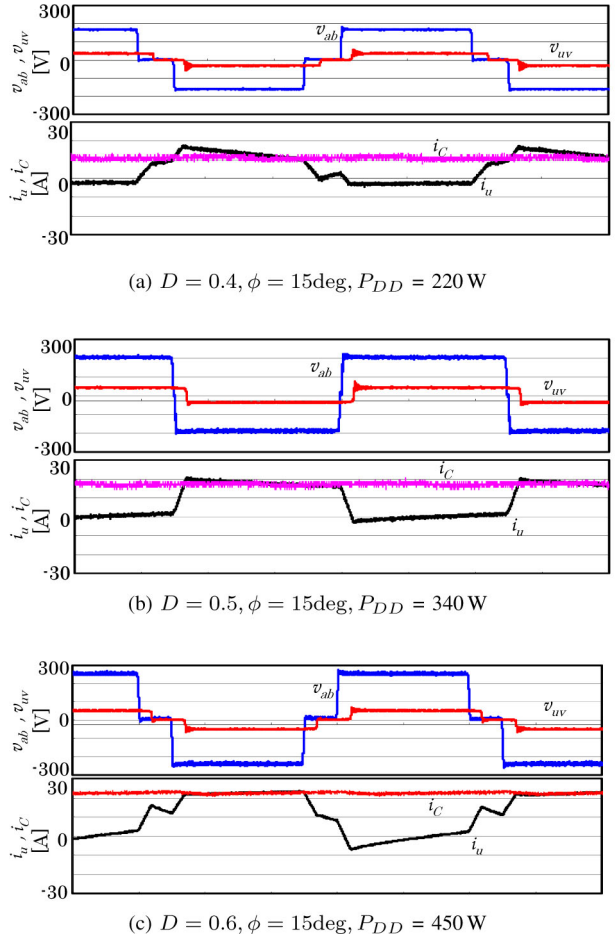

(a) $D = 0.4, \phi = 15$deg, P_{DD} = 220 W

(b) $D = 0.5, \phi = 15$deg, P_{DD} = 340 W

(c) $D = 0.6, \phi = 15$deg, P_{DD} = 450 W

Fig. 9 Experimental waveforms of the proposed circuit, port C and port D are dc sources set as $V_C = 20$ V, $V_D = 100$ V; port B and port A are opened.

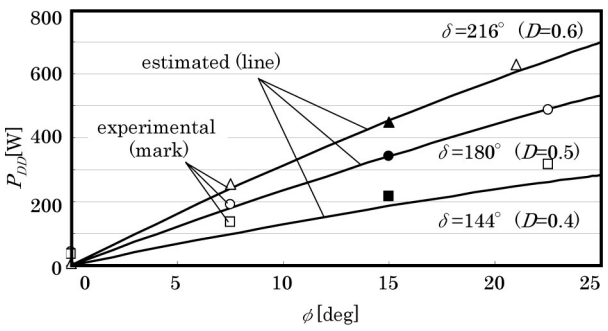

Fig. 10 Power-transferred value P_{DD} from port C to port D vs. phase shift angle ϕ. The three dark symbols are the result of Fig. 9.

Figure 11 plots the measured converter efficiency. Figure 11(a) shows the conversion efficiency of each function, and these values are above 90% over a wide range of output power. The efficiency of the boost converter is 90.3% at P_B = 200 W, 96.2% at P_B = 600 W, and that of the isolated dc-dc converter is 92.7% at P_B = 200 W, 91.2% at P_B = 600 W. Figure 11(b) shows the total efficiency of the hybrid mode. In this mode, a part of P_B is provided from port A, and the other part is provided from port D, under the constant load configuration P_B = 400 W. The distribution factor k_r is defined as $k_r = P_{DD} / P_B \times 100$, and rated at 0 – 100%. The total efficiency η is equal to $P_B / (P_C + P_D) \times 100$ and reaches a maximum 97% at k_r = 50%. Because the proposed converter reduces the number of components, the total loss and consumption are improved drastically. If the same power is given to port B by using the conventional boost converter and the isolated dc-dc converter, the total efficiency is lower than that of the hybrid mode. For example, in the estimate from the result of Fig. 11(a), the total efficiency is only 91% for the same distribution factor.

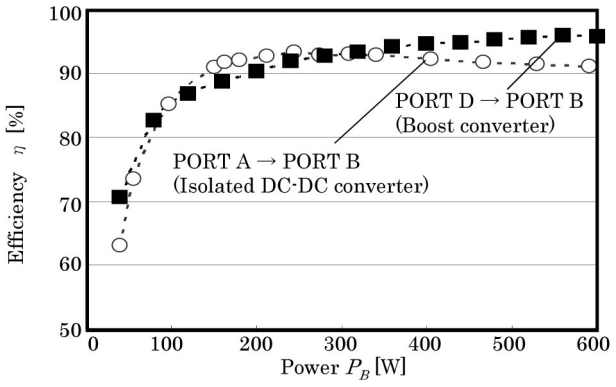

(a) Efficiency of each function

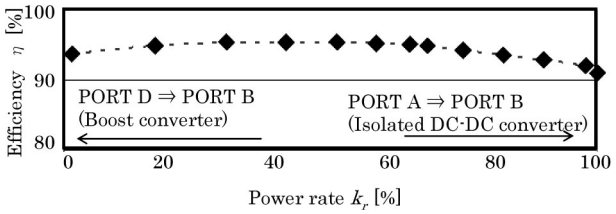

(b) Efficiency of hybrid mode at P_B=400 W

Fig. 11 Measured efficiency of each function. When measuring the isolated dc-dc converter, the input power source is connected to port A and V_A = 50 V, V_B = 250 V, and port C and port D are opened. When measuring the boost converter, the input power source is connected to port D and V_B = 250 V, V_D = 100 V, and port A and port D are opened. When measuring the hybrid mode, the input power source is connected to ports A and D and V_A = 50 V, V_B = 250 V, V_D = 100 V, and port C is opened.

4. 2 System Example and Simulation Result

As one example of using the proposed converter, an electric vehicle power system and its controller are shown in **Fig. 12**. The motor MG connects to port B, the main battery $BATT_s$ connects to port B, and the system battery $BATT_m$ connects to port C. A solar panel is placed at port A with a contactor SW for charging two batteries. In Fig. 12, there are two feedback controllers in one system. To drive the vehicle, contactor SW turns off, the secondary boost converter controls the voltage of port B to command V_B^* from the motor MG by adjusting δ with the PI controller. Depending on the usage of the batteries, the transferred power between the primary and the secondary P_{DD} is controlled by another PI controller. In a parking situation, the contactor SW is turned on, and $BATT_m$ and $BATT_s$ are changed by controlling P_{DD}. The feedforward values δ_{ff} and ϕ_{ff}, estimated by Eqs. (1) and (10), have a role in reducing the interference between P_{DD} and V_B.

Figure 13 shows the simulation waveforms of Fig. 12. The parameters are the same as those for the

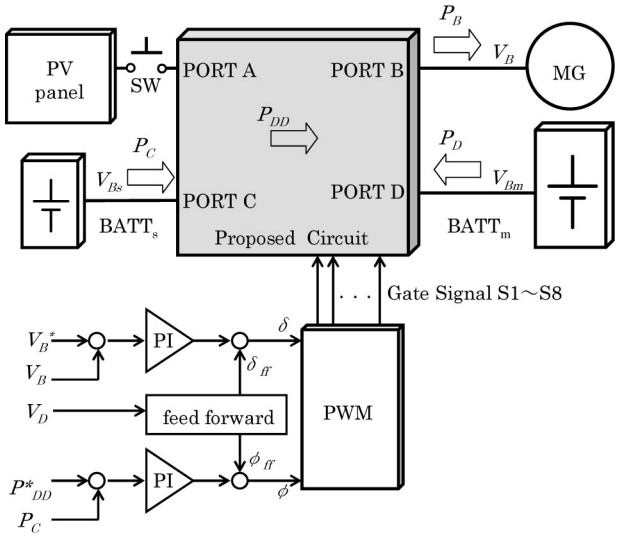

Fig. 12 System example of the proposed circuit. This case supposes a motor drive system based on Fig. 1, but the three blocks "CONVERTER A – C" are replaced by ONE proposed converter.

experimental circuit configuration, as listed in Table 4. In the period $t_1 \le t \le t_2$, P^*_{DD}, 0 W to 250 W, transfers power from port C to port D. The feedback controller adjusts ϕ by approximately 20 degrees and keeps P_{DD} as the command value in $t_2 \le t \le t_3$. In the next period $t_3 \le t \le t_4$, load P_B increases from 0 W to 600 W, and the port D supply is P_D = 350 W in accordance with the relationship, $P_B = P_{DD} + P_D$. In the last period $t_5 \le t \le t_6$, the command of output voltage V_B^* increases from 150 V to 300 V, then the feedback controller adjusts δ from 110 degrees to 250 degrees by following Eq. (1). In this case, the controller decreases phase angle ϕ to keep P_{DD} = 250 W under Eq. (10), that is, non-interacting control is achieved in this converter.

5. Conclusion

In this paper, a multi-port converter formed by inversely coupled inductors and center-tapped was presented. For adjusting the duty ratio and the phase angle of full-bridged switches, it is possible to integrate boost conversion and isolated dc-dc converter function and connect four dc sources/load in one circuit. The theoretical analysis and the experimental results verified the multi-functionality of the magnetic components and the converter operation, and it was also shown that the proposed converter has the ability to downsize and improve energy consumption of complex dc power systems. In addition, an example of system utilization was shown, and the simulation result confirmed that it is able to replace discrete converters with one proposed converter without any difficulty in terms of control performance. This converter is suitable for multi-input multi-output systems, such as electric vehicle systems and renewable energy systems.

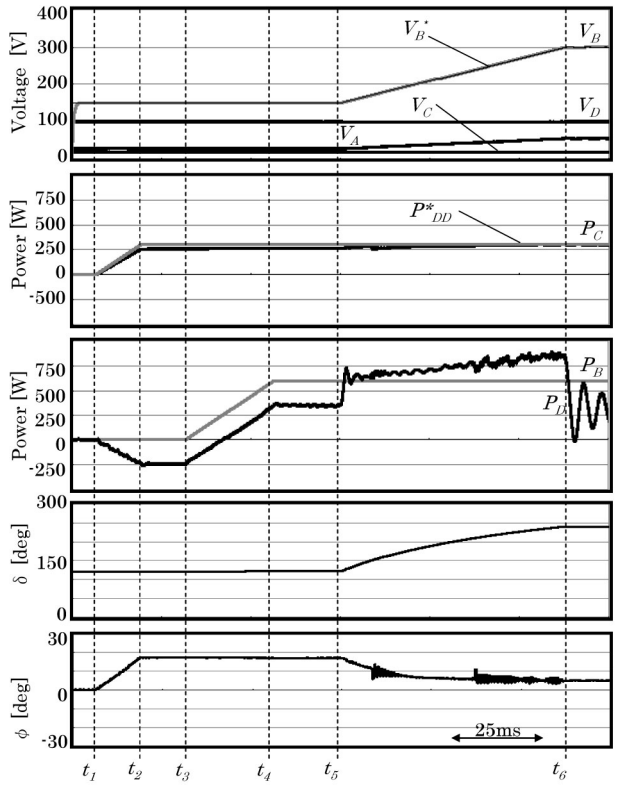

Fig. 13 Simulation results of Fig. 12. In this simulation, the independence of two factors, V_B and P_{DD}, is confirmed by the wavefroms.

REFERENCES

(1) Zhang, W., Dong, D., Cvetkovic, I., Lee, F. C. and Boroyevich, D., "Lithiumbased Energy Storage Management for DC Distributed Renewable Energy System", *ECCE* (2011), pp. 3270-3277.

(2) Barton, J. P. and Infield, D. G., "Energy Storage and Its Use with Intermittent Renewable Energy", *IEEE Trans. Energy Converters*, Vol. 19, No. 6 (2004), pp. 441-448.

(3) Snyder, K., Yang, X. and Miller, T., "Hybrid Vehicle Battery Technology; The Transition from NiMH to Li-Ion", *SAE Tech. Pap. Ser.*, No. 2009-01-1385 (2009)

(4) Kassakian, J. G., "Automotive Electrical Systems; The Power Electronics Market of the Future", *Applied Power Electronics Conference APEC 2010*, Vol. 1 (2010), pp. 3-9.

(5) Tshukuda, M. and Omura, I., "Demonstration of High Output Power Density (30 W/cc) Converter Using 600 V SiC-SBD and Low Impedance Gate Driver," *IPEC 2005* (2005), pp. 1184-1189.

(6) Simanjorang, R. et al., "A High Output Power Density 400/400 V Isolated DC/DC Converter with Hybrid Pair of SJ-MOSFET and SiC-SBD for Power Supply of Data Center", *Applied Power Electronics Conference APEC 2010* (2010), pp. 648-653.

(7) Eckardt, B. et al., "Automotive Powertrain DC/DC Converter with 25 kW/cc by Using SiC Diode", *Integrated Power Systems CIPS*, CD-ROM (2006).

(8) Badstuebner, U., Biela, J. and Kolar, J. W., "Design of a 99%-efficient, 5 kW, Phase-shift PWM DC-DC Converter for Telecom Applications", *Applied Power Electronics Conference APEC 2010* (2010), pp. 773-780.

(9) Zhao, C., Round, S. D. and Kolar, J. W., "An Isolated Three-port Bidirectional DC-DC Converter with Decoupled Power Flow Management", *IEEE Trans. on Power Electronics*, Vol. 23, No. 5 (2008), pp.2443-2453

(10) Sun, P. and Lai, J.-S., "Efficiency Evaluation of a

55 kW Soft-switching Module Based Inverter for High Temperature Hybrid Electric Vehicle Drive Application", *Applied Power Electronics Conference APEC 2010* (2010), pp. 773-780 .
(11) Tao, H. et al., "Family of Multiport Bidirectional DC-DC Converters", *Electric Power Applications, IEE Proceedings*, Vol. 153, No. 3 (2006), pp. 451-458.
(12) Tao, H. et al., "Multi-input Bidirectional DC-DC Converter Combining DC-link and Magnetic-coupling for Fuel Cell Systems", *Proc. IEEE Ind Appl. Conf.*, Vol. 3 (2005), pp. 2021-2028.
(13) Su, G.-J. and Peng, F. Z., "Low Cost, Triple-voltage Bus DC/DC Converter for Automotive Application", *Applied Power Electronics Conference APEC 2005*, Vol. 2 (2005), pp. 1015-1021.
(14) Sasaki, S., "Toyota's Newly Developed Hybrid Powertrain", *Proceedings of ISPSD 1998* (1998) pp. 17-22.
(15) Okamura, M. et al., "Development of Hybrid Electric Drive System Using a Boost Converter", *EVS20 2003* (CD-ROM) (2003).
(16) Hamada, K. et al., "Low Loss High Ruggedness PT-IGBT for 500 V Variable Voltage Hybrid System", *IPEC 2005* (2005), pp. 315-321.
(17) Pavlovsky, M. et al., "Bi-directional Buck/boost DC-DC Converter with Ultra High Efficiency Based on Improved SAZZ Topology", *ECCE 2009* (2009), pp. 1783-1790.
(18) Wong, P., Lee, F. C., et al., "Performance Improvements of Interleaving VRMs with Coupling Inductors", *IEEE Trans. on Power Electronics*, Vol. 16, No. 4 (2001), pp. 499-507.
(19) Hartnett, K. J., Wong, P., Lee, F. C., et al., "A Novel Modeling Concept for Multi-coupling Core Structures", *IPEC 2010*, Vol. 1 (2010), pp. 2941-2948.
(20) Hirakawa, M. et al., "High Power DC/DC Converter Using Extreme Close-coupled Inductors Aimed for Electric Vehicles", *IPEC 2010*, Vol. 1 (2010), pp. 2941-2948.
(21) Peng, F. Z., Li, H., Su, G.-J. and Jack, S. L., "A New ZVS Bidirectional DC-DC Converter for Fuel Cell and Battery Application," *IEEE Trans. on Power Electronics*, Vol. 19, No. 1 (2004), pp. 54-65.
(22) Inoue, S. and Akagi, H., "A Bi-directional DC/DC Converter for an Energy Storage System", *Applied Power Electronics Conference APEC 2007* (2007), pp. 761-767.
(23) Biela, J. et al., "Bi-directional Isolated DC-DC Converter for Next Generation Power Distribution; Comparison of Converters Using Si and SiC Devices", *IEEJ Trans. D*, Vol. 128, No. 7 (2008).

Masanori Ishigaki
Research Fields:
- Power Electronics
- HV/EV Electric Drive System

Academic Society:
- The Institute of Electrical Engineers of Japan

Awards:
- IEEJ Best Presentation Award, 2007
- IEEE IPEC Second Paper Prized Award, 2010
- IEEE APEC Outstanding Presentation Award, 2012
- IEEJ Best Presentation Award, 2012
- IEEJ Encouraging Prize Award, 2012

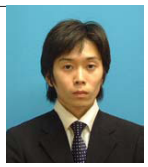

Kenichi Ito
Research Fields:
- Power Electronics
- Power Devices
- Electrical Circuit

Academic Societies:
- The Japan Society of Applied Physics
- The Institute of Electrical Engieers of Japan

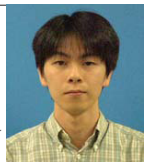

Shuji Tomura
Research Field:
- Research and Development of Hybrid Powertrain System, Control, and Battery Management System

Academic Societies:
- The Society of Instrument and Control Engineers
- The Society of Automotive Engineers of Japan

Takaji Umeno
Research Fields:
- Power Electronics
- HV/EV Electric Drive System

Academic Degree: Dr.Eng.

Academic Societies:
- The Institute of Electrical and Electronics Engineers
- The Institute of Electrical Engineers of Japan
- The Society of Instrument and Control Engineers
- The Society of Automotive Engineers of Japan

Award:
- IEEE/IES Outstanding Paper Award, 1994
- Robomec'94 Best Paper Poster Award, 1995
- R&D 100 Award, 1997
- SICE Chubu Chapter Award for Outstanding Technology, 2002
- Paper Award of AVEC '02, 2002

